Improvements to the Finite-Difference Time-Domain Method for Calculating the Radar Cross Section of a Perfectly Conducting Target

CYNTHIA M. FURSE, SATNAM P. MATHUR, MEMBER, IEEE, AND OM P. GANDHI, FELLOW, IEEE

Abstract—**The finite-difference time-domain (FDTD) method has been used extensively to calculate scattering and absorption from both dielectric objects and perfectly conducting objects. Several improvements to the FDTD method for calculating the radar cross section (RCS) of a perfectly conducting target are presented in this paper. Sinusoidal and pulsed FDTD excitations are compared to determine an efficient method of finding the frequency response of targets. The maximum cell size, the minimum number of external cells, and a new method to eliminate field storage in the shielded internal volume of perfect conductors to reduce the computer storage requirements of FDTD are discussed. The magnetic field dc offset induced by surface currents on perfectly conductive objects is observed and its effects removed by postprocessing to achieve convergence of RCS calculations. RCS calculations using the FDTD method in two dimensions are presented for both square and circular infinite cylinders illuminated by both TE and TM polarized plane waves. The RCS of a metal cube in three dimensions is also presented. Good agreement between FDTD calculations and theoretical values is achieved for all cases, and parameters necessary to achieve this agreement are examined.**

I. Introduction

THE FINITE-DIFFERENCE time-domain (FDTD) method has been used extensively to calculate scattering and absorption from both dielectric objects and perfectly conducting objects. Applications of this method include human body dosimetry studies for electromagnetic safety [1] and hyperthermia [2], analysis of microstrip circuits [3], [4], studies of electromagnetic pulse (EMP) interaction with targets [5], and radar cross section (RCS) calculations [6].

The complete RCS signature of a target is described by the frequency response of the target illuminated by plane waves from all possible physical angles. Realistic targets are frequently very large (of the order of 10λ or more) and are often largely made up of highly conductive materials. In this study several improvements to the FDTD method for calculating the RCS of a perfectly conducting target are presented. The efficiencies of sinusoidal and pulsed FDTD excitations in determining the frequency response of a target are compared in Section II. Methods to reduce the large computer storage requirements of FDTD are discussed in Section III. The maximum cell size and the minimum number of external cells are studied to determine the minimum model size, and a new method to eliminate field storage in the shielded internal volume of perfect conductors is demonstrated. In Section IV a dc offset in the magnetic fields around highly conductive objects is observed to cause oscillation in the frequency-domain calculations and hence in the RCS calculations. Methods to remove these oscillations in both continuous wave (CW) and pulsed FDTD through postprocess averaging are shown to achieve proper convergence of RCS calculations. RCS calculations using the FDTD method in two dimensions are presented for both square and circular infinite cylinders illuminated by both TE and TM polarized plane waves. The RCS of a metal cube in three dimensions is also presented. Good agreement between FDTD calculations and theoretical values is achieved for all cases, and parameters necessary to achieve this agreement are examined.

Manuscript received October 6, 1989; revised March 15, 1990. This work was supported by the Sandia National Laboratories under Contract 63-9099 and by the Radar Systems Division of the Hughes Aircraft Company.

C. M. Furse and O. P. Gandhi are with the Department of Electrical Engineering, University of Utah, Salt Lake City, UT 84112.

S. P. Mathur was with the Department of Electrical Engineering, University of Utah, Salt Lake City, UT 84112. He is now with the ERC toServices Corporation, Gaithersburg, MD.

IEEE Log Number 9036155.

II. Comparison of CW and Pulsed FDTD

Calculation of the complete RCS signature of a target requires computation of its frequency response. This can be done using the FDTD method in one of two ways. First, the CW FDTD solution may be found in the steady state for sine wave illumination [6]. This method requires an individual FDTD run for every frequency of interest. An alternative approach is to use FDTD with a time-limited pulsed plane wave excitation (pulsed FDTD) and take the Fourier transform of the time-domain waveforms to obtain the frequency response of the target. This method provides the complete frequency response from a single FDTD run.

The major advantage of pulsed FDTD over CW FDTD is that pulsed FDTD can obtain results over a broad frequency band from a single FDTD run with little or no

0018-9480/90/0700-0919$01.00 ©1990 IEEE

more computational effort than that required for a single CW FDTD run at the highest frequency of interest. The modeling requirements (cell size and model size) for the pulsed FDTD are identical to those required for the highest frequency CW FDTD run. The cell size is chosen for both methods on the basis of the minimum wavelength in the model (λ_{min}). This is a function of the electrical properties of the target and the highest incident frequency. The incident plane wave pulse is chosen to be band limited to the highest frequency of interest, so that the highest frequency in pulsed FDTD is identical to the highest frequency (the only frequency) in CW FDTD. Since both the electrical properties of the target and the highest frequency to be modeled are identical, the physical models are also identical for pulsed FDTD and CW FDTD.

Two kinds of pulses are commonly used for pulsed FDTD: Gaussian [3] and raised cosine [4]. The raised cosine is broader in time, and the frequency spectra of the two pulses are very similar. The raised cosine pulse was used in this study because its width in time is identical to one period of the sinusoidal excitation used for CW FDTD. The raised cosine pulse is given by

$$Ez(t) = \begin{cases} 1-\cos(2\pi F_b t), & t \leq 1/F_b \\ 0, & t > 1/F_b. \end{cases} \quad (1)$$

The pulse used for most test cases in this study has $F_b = 4$ GHz. If a cell size of $\Delta x = \lambda_{min}/20$ is used and the time step is chosen so that $\Delta t = \Delta x/2c_0$ for generous stability of the FDTD algorithm [6], then this pulse is about 40 time steps broad, as is one period of the CW sinusoid. A Gaussian pulse with the same bandwidth could be as narrow as 20 time steps [3]. Convergence is determined for pulsed FDTD when the pulse has decayed to 0 at all points in the FDTD problem space. Similarly, convergence for CW FDTD is determined when the sinusoid has reached a steady-state oscillation at every point. In all of our calculations, we observed that a time duration equal to that needed for highest frequency CW FDTD runs was sufficient to obtain converged solutions for the pulse. This result is most interesting since we would have expected to need a longer time-domain representation because of the lower frequency components contained in the pulse. These lower frequencies would have taken longer to converge had CW FDTD runs been made at these frequencies. In future work it would be interesting to study this observation in greater depth because of the high numerical efficiency that this implies.

CW and pulsed FDTD differ in the method used to determine the magnitude and phase of the frequency-domain solution. In CW FDTD, the envelope and the phase are determined directly from the time-domain steady-state waveforms. In this study a difference-based peak detection scheme was used for this purpose. Three successive points in time were compared to determine when a peak had been reached. The peak value (magnitude of the envelope) was then recorded as the center of the three values. The phase was determined by subdividing one period (360°) by the number of time steps in one period of the sinusoid. For a cell size of $\lambda/20$ (time step corresponding to $\lambda/40$), this subdivision is 9°. The phase was recorded as the nearest subdivision when the peak was reached, so a phase error of $\pm 4.5°$ for a $\lambda/20$ cell size was inherent in this method. This simple method was chosen for this study to make the computational times for CW and pulsed FDTD as nearly equivalent as possible. More accurate methods of magnitude and phase detection could be used, but would require more computer storage and computation time.

This simple envelope and phase detection algorithm requires storage of the positive and negative peaks of the sinusoid and the integer associated with the phase. This gives a storage overhead of two real and one integer values for each field component at every cell where the frequency response is calculated. For RCS calculations, the frequency response is needed for all cells on an enclosed volume surrounding the scatterer in three dimensions or an enclosed surface in two dimensions. For 3-D calculations, this overhead is of the order of $18N^2$ in addition to the basic FDTD storage requirement of $6N^3$, where N is the number of cells on a side of the problem space.

The magnitude and phase of the envelope are determined in pulsed FDTD by taking the discrete Fourier transform of the time-domain waveforms. The discrete Fourier transform (DFT) is given by

$$G(k\Delta f) = \Delta t \sum_{n=0}^{N-1} g(n\Delta t) \exp\left(\frac{-j2\pi kn}{N}\right), \quad k = 0,1,2,\ldots,\mathrm{NF} \quad (2)$$

where $g(n\Delta t)$ is the discrete time-domain field value (from FDTD), n is the time step index, N is the length of the DFT (number of available frequencies), $\Delta f = 1/(N\Delta t)$ is the frequency resolution, and k is the frequency index. The magnitude and phase of $G(k\Delta f)$ are equivalent to the magnitude and phase of the steady-state envelope for the frequency $F = k\Delta f$. The summation in (2) is updated at every FDTD time step, and the final values are normalized by the DFT of the incident pulse. The complex value $G(k\Delta f)$ must be stored for every field component at each frequency of interest and at every cell where the frequency response is calculated. The storage overhead for this case is of the order of $12N^2 * \mathrm{NF}$, where NF is the number of frequencies being examined. For single frequency calculation, the storage overhead for pulsed FDTD is smaller than for CW FDTD. The overhead for pulsed FDTD increases linearly with the number of frequencies. Since this overhead is small compared to the basic FDTD storage, both methods require very nearly the same computer storage.

It is worth noting that the DFT algorithm is more efficient than the fast Fourier transform (FFT) algorithm for computing the frequency response from pulsed FDTD because only a limited number of the available frequen-

cies are of interest. Consider, for example, a 4 GHz band-limited raised cosine pulse with a cell size of $\lambda_{min}/20$. If Δf is chosen to be 0.125 GHz, then the number of available frequencies is $N = 1280$. Frequencies above 4 GHz are not significant, however, because of the band limitation of the pulse, so only a maximum of 32 frequencies (not counting dc) may be of interest. Since N must always be greater than or equal to the number of FDTD time steps, only a small portion of these N frequencies will be significant. The DFT algorithm is more efficient than the FFT algorithm for cases such as this, where only a small portion of the available frequency spectrum is actually computed.

Results calculated using CW and pulsed FDTD were found to be nearly identical. The bistatic RCS of a square, perfectly conducting infinite cylinder in two dimensions was calculated using FDTD with a CW frequency of 4.25 GHz or a raised cosine with $F_b = 4.25$ GHz. A cell size of $\Delta x = \lambda_{min}/20\pi$ was used for comparison with previously published results [7]. The FDTD space includes the scatterer surrounded by a total field region and then a scattered field region and the absorbing boundary as in [7]. Second-order Mur boundary conditions on the electric fields were used to absorb outgoing waves [8], and the absorbing boundary was located 15 cells from the cylinder. The cylinder was modeled with 20 cells on a side. The solution converged well after 350 time steps for both methods. The frequency-domain scattered fields were computed during time stepping on a square contour five cells from the outer boundary of the model, transformed to the far field, and integrated using trapezoidal integration to find the bistatic RCS. Adjustment of the magnetic field offset as described in Section IV was used. The bistatic RCS of the square cylinder is shown in Fig. 1 for both CW (solid line) and pulsed FDTD (solid dots) solutions. Both methods agree with previously published results [7]. A maximum variation between CW and pulsed FDTD solutions of 3% was observed, and the average variation was less than 2%.

Computation times for CW and pulsed FDTD were compared for the square cylinder test case described above. Table I shows a comparison of CPU time required in each portion of the CW and pulsed codes for a single-frequency analysis (at $f = 4.25$ GHz) and for a complete frequency response analysis (17 frequencies up to $f = 4.25$ GHz, $\Delta f = 0.25$ GHz). The computation time required for the single-frequency run was nearly identical for CW and pulsed FDTD. To obtain the bistatic RCS for 17 frequencies, however, the CW FDTD would have to be rerun 17 times. If the model is unchanged, this would require 17 times as much computational time as the single-frequency run. Some savings could be achieved by modeling the cylinder with a coarser grid at lower frequencies. With these savings, it is estimated that the RCS could be calculated for 17 frequencies with about nine times the computational time required for single-frequency calculations. It should be noted that the use of coarser grids might be prohibited by the small physical

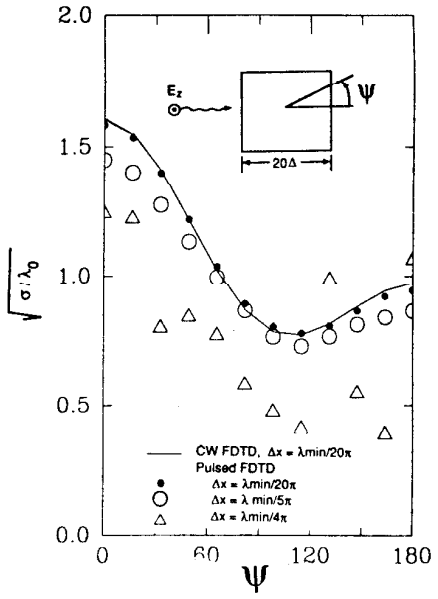

Fig. 1. Bistatic RCS of a square, perfectly conducting infinite cylinder: comparison of CW and pulsed FDTD. Values are shown for pulsed FDTD with cell sizes ranging from $\Delta x = \lambda_{min}/20\pi$ to $\Delta x = \lambda_{min}/4\pi$. $f = 4.25$ GHz.

TABLE I
COMPARISON OF CPU TIME FOR CW AND PULSED FDTD FOR BISTATIC RCS OF SQUARE PERFECTLY CONDUCTING INFINITE CYLINDER (CALCULATED RCS SHOWN IN FIG. 1)

Values given in cpu seconds on Gould 9080	1 frequency		17 frequencies	
	CW	Pulse	CW	Pulse
FDTD	64.2	64.2		64.2
Envelope, Phase/ dFT	8.1	7.8	*Requires 17 individual runs; (a) coarser grid at lower frequencies (b) model unchanged	192.3
RCS (14 times)	4.8	4.8		6.1
Total	77.1	76.8	(a) 700* (b) 1310.7	262.6

*Estimated value

characteristics of certain scatterers (thin plates, struts, slots, etc.). Multiple-frequency analysis using pulsed FDTD, on the other hand, would require only the single FDTD run and additional DFT and RCS calculations for each additional frequency. These additional computations increased the computation time of the pulsed FDTD run by about 3.5 times, as compared with nine to 17 times for the CW FDTD run. Overall, the CW FDTD would require three to five times as much computation time as the pulsed FDTD for calculation of the RCS at 17 frequencies.

Savings of this sort are not exclusive to this test case. In general, CW and pulsed FDTD require very nearly the same amount of computation time for a single-frequency

analysis, and pulsed FDTD is significantly more efficient than CW FDTD for multiple-frequency analysis. Memory requirements for pulsed FDTD are virtually identical to those of the highest frequency CW FDTD run, and the two methods yield nearly identical frequency-domain results. It should be noted that to conserve time in all test cases in this study, the envelope and phase were calculated only for the surface points used in the near-to-far field transformation. For the above test cases, a square contour 41 cells on a side was used, requiring envelope and phase computation at 160 points.

One limitation of using pulsed FDTD with the traditional FDTD algorithm is that the electrical properties of the scatterer (ϵ_r, μ_r, and σ) are assumed not to vary significantly within the frequency band of interest. This limitation may be overcome in one of two ways. Either the pulsed FDTD solution may be used one frequency at a time or a modified FDTD algorithm for materials with frequency-dependent properties may be used [9].

III. Minimization of Computer Storage Requirements

Realistic targets for FDTD RCS computation may span over ten wavelengths and require over a million cells for three-dimensional modeling. Storage for models of this magnitude may exceed seven megawords. It is desirable to minimize the storage required in order to maximize the target size that can be modeled with a given storage limit. Also, since the computation time for FDTD is directly proportional to the number of cells in the model, minimizing the model size maximizes the overall efficiency of the algorithm. In this section, the use of the maximum cell size and the minimum spacing between the target and the absorbing boundary are discussed to minimize the model size. A new method to eliminate field storage in the shielded internal volume of metallic scatterers is also presented to further reduce memory requirements.

A. Maximum Cell Size

The maximum cell size for FDTD modeling, Δx, has been suggested to be between $\lambda_{min}/10$ and $\lambda_{min}/20$ based on the numerical error in the spatial derivatives [6]. In practice, however, researchers have used cell sizes ranging from $\lambda_{min}/4$ [6] to $\lambda_{min}/200$ [7]. In order to determine what cell sizes are practical for RCS calculations of simple scatterers, comparisons of different cell sizes were made for a square metal cylinder illuminated by a TM polarized plane wave, a metal cube, and a circular metal cylinder illuminated by both TM and TE polarized plane waves.

To determine the maximum usable cell size for square and rectangular targets, the bistatic RCS of the square metal cylinder discussed in Section II was computed using pulsed FDTD with cell sizes ranging from approximately $\lambda_{min}/60$ to $\lambda_{min}/10$. The square cylinder was first modeled with 20 cells on a side and a cell size of $\Delta x = \lambda_{min}/20\pi$. The cylinder was then modeled with five cells on a side and a cell size of $\Delta x = \lambda_{min}/5\pi$. The average deviation between these results and those calculated with $\Delta x = \lambda_{min}/20\pi$ is about 6.5%. The cylinder was finally modeled with four cells on a side and a cell size of $\Delta x = \lambda_{min}/4\pi$. The average deviation between these results and those calculated using $\Delta x = \lambda_{min}/20\pi$ is about 34%, with a maximum deviation of 60% at some angles.

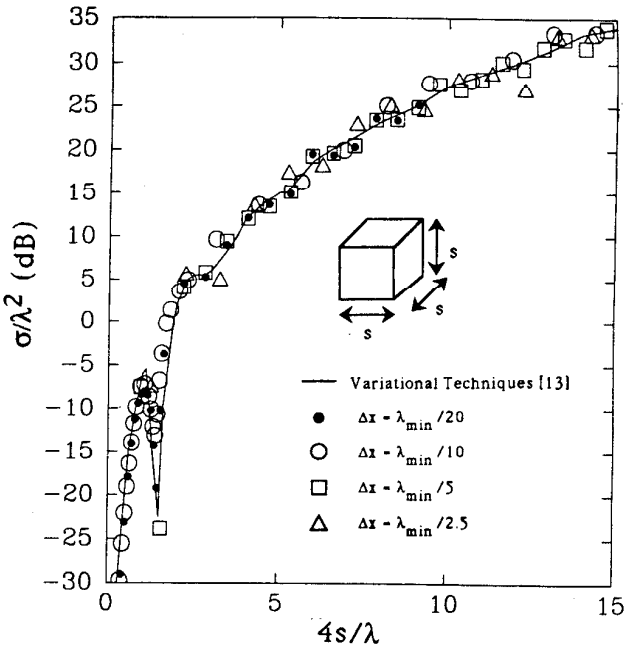

Fig. 2. Backscattered RCS of a perfectly conducting cube: comparison of cell size.

A similar test was made to determine the maximum allowable FDTD cell size for a metal cube in three dimensions. A TM polarized raised cosine pulse plane wave band limited to 4 GHz was used to illuminate the cube. For cell sizes of $\Delta x = \lambda_{min}/20$, $\lambda_{min}/10$, and $\lambda_{min}/5$, the cube was modeled with 50 cells on a side; for $\Delta x = \lambda_{min}/2.5$, the cube was modeled with 20 cells on a side. All models had nine cells between the cube and the absorbing boundary. Results are shown in Fig. 2 for the backscattered RCS of the cube as a function of wavelength and cell size and are compared to results from variational techniques [13]. All values shown for a given Δx were calculated from a single pulsed FDTD run. It was found from these test cases that a cell size as low as $\lambda_{min}/5$ is sufficient to compute the RCS of cubical metal targets. It appears that the poor performance of the square cylinder test case at these cell sizes was the result of a very small model rather than large cell size.

The maximum usable cell size was then examined for a circular metal cylinder illuminated by a TM polarized plane wave. Since the boundary of this and other curved targets is modeled by a stepped approximation rather than an exact boundary, it was expected that a slightly smaller cell size must be used to obtain accurate result A TM polarized plane wave with a 4 GHz band limited raised cosine pulse was used to illuminate the cylinder. For a cell size of $\Delta x = \lambda_{min}/60$ the cylinder was modeled

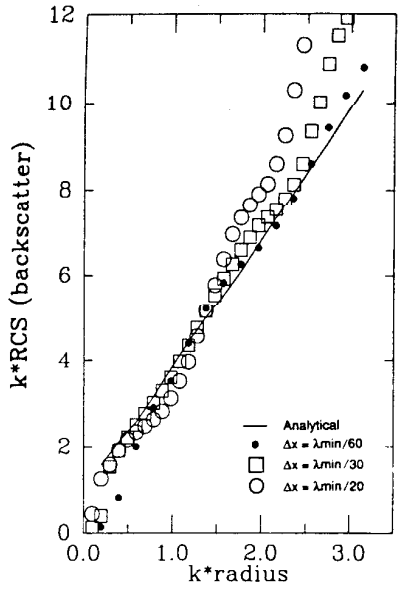

Fig. 3. Backscattered RCS of a circular, perfectly conducting infinite cylinder (TM polarization): comparison of cell size. Radius = 0.0375 m, maximum frequency = 4 GHz.

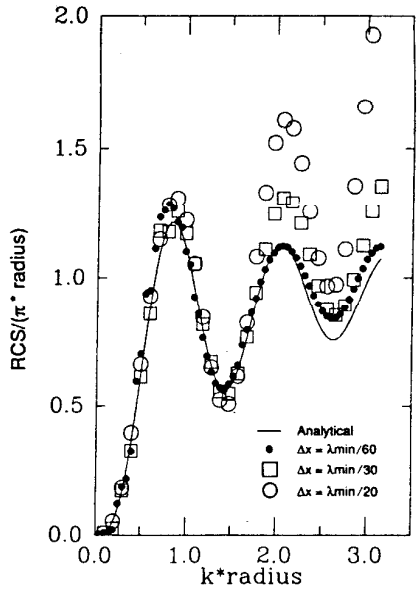

Fig. 4. Backscattered RCS of a circular, perfectly conducting infinite cylinder (TE polarization): comparison of cell size. Radius = 0.0375 m, maximum frequency = 4 GHz.

with a 60 cell diameter, for $\Delta x = \lambda_{min}/30$ the cylinder was modeled with a 30 cell diameter, and for $\Delta x = \lambda_{min}/20$ the cylinder was modeled with a 20 cell diameter. Results are shown in Fig. 3 for the backscattered RCS of the circular metal cylinder as a function of frequency ($k = 2\pi F/c$) and cell size. Analytical results were calculated from the Bessel function expansion of the fields around the cylinder and compared to published results [11]. The average deviation between theoretical and FDTD calculated results is 3.7% for $\Delta x = \lambda_{min}/60$, 4.5% for $\Delta x = \lambda_{min}/30$, and 18.1% for $\Delta x = \lambda_{min}/20$. In general, a cell size between $\lambda_{min}/20$ and $\lambda_{min}/30$ is sufficient to compute the RCS of TM polarized circular metal cylinders to within 10% error. As expected, a slightly smaller cell size must be used to model curved rather than square targets. It is likely that the use of boundary fitted coordinates as in [6] and [14] may relax this requirement.

The maximum allowable cell size was also examined for a circular metal cylinder illuminated by a TE polarized plane wave. It is expected that the circular cylinder illuminated by a TE polarized plane wave would be more susceptible than a TM illuminated cylinder to errors induced by step modeling of the curved surface because of the existence of creeping waves in this polarization. A TE polarized raised cosine pulsed plane wave band limited to 4 GHz was used to illuminate the cylinder. The model parameters used were identical to those used for the TM illuminated circular cylinder described above. Results are shown in Fig. 4 for the backscattered RCS of the circular metal cylinder as a function of frequency ($k = 2\pi F/c$) and cell size. Analytical results were calculated from the Bessel function expansion of fields around the cylinder and verified by comparison with [11]. The average deviation between analytical and FDTD results is 6.8% for $\Delta x = \lambda_{min}/60$, 10.1% for $\Delta x = \lambda_{min}/30$, and 26.6% for $\Delta x = \lambda_{min}/20$. A cell size of about $\lambda_{min}/30$ is sufficient to compute the RCS of TE polarized circular cylinders to within 10% error. As expected, a slightly smaller cell size must be used to model a circular cylinder illuminated by TE rather than TM polarization.

In conclusion, it is desirable to model a target with the largest possible cell size to minimize the number of FDTD cells required. Appropriate cell sizes to model the RCS within 10% error were found to be as low as $\lambda_{min}/5$ for square/rectangular objects, $\lambda_{min}/20$ to $\lambda_{min}/30$ for curved objects illuminated by TM polarization, and about $\lambda_{min}/30$ for curved objects illuminated by TE polarization.

B. Minimum Number of External Cells

The total number of FDTD cells can be minimized by using the largest possible cell size to model the target and the minimum number of cells external to the target. The required number of cells between the target and absorbing boundary depends on the quality of the boundary condition used, the size of the target and its scattering nature, and the size of the cells. This idea has been discussed in general by Moore [12], among others, but specific target–boundary separations have not been discussed in detail. Separations ranging from $0.17\lambda_{min}$ to $0.32\ \lambda_{min}$ and eight cells to 20 cells have been used in practice [6].

Tests to determine the minimum practical spacing between the target and the absorbing boundary were made on a square perfectly conducting infinite cylinder. Outgoing waves were eliminated on the absorbing boundary using second-order Mur boundary conditions on the electric field [8]. This boundary condition is expected to achieve complete absorption of waves normally incident

on the boundary, and a 3% reflection is expected for waves incident at 45°. The square cylinder was used as the test case because of the expectation that a significant portion of the fields will be scattered in off-normal angles of incidence, thereby making it a worst-case test case. A raised cosine plane wave pulse with $F_b = 4.25$ GHz was used to illuminate the cylinder. The square was first modeled with 15 cells between the cylinder and the absorbing boundary, $\Delta x = \lambda_{\min}/5\pi$, and five cells on a side. The bistatic RCS of the cylinder at 4.25 GHz is shown in Fig. 1 (open circles). The spacing between the cylinder and the absorbing boundary was then reduced to six cells. Results for the bistatic RCS at 4.25 GHz were altered by about 2%, so it appears that six cells provide sufficient spacing between the cylinder and the absorbing boundary. This is a distance of $0.38\lambda_{\min}$. Reducing the boundary layer from 15 cells to six cells for the $\Delta x = \lambda_{\min}/20\pi$ calculation in Fig. 1 altered the RCS by about 2%. This is a spacing of 0.095 $\lambda_{\min}$. No fewer than six cells could be used in the algorithm as we have programmed it, so smaller spacings were not examined. A minimum spacing of six cells is required because three cells are required to absorb the outgoing waves at the boundary, one cell is required to store scattered fields which are used to calculate RCS, one cell is required to insert the incident plane wave, and one cell is required to properly match the boundary conditions on the surface of the scatterer.

A minimum spacing of six cells between the target and the absorbing boundary was not sufficient to provide good results for a metal cube in three dimensions, however. Backscattered RCS's of the metal cube for cell size ranging from $\Delta x = \lambda_{\min}/20$ to $\lambda_{\min}/2.5$ are shown in Fig. 2. These models were found to require eight to nine cells between the cube and the absorbing boundary to achieve good agreement between analytical and calculated values.

It appears in general that a cell spacing of six to nine cells between the target and the absorbing boundary is sufficient to adequately absorb the outgoing waves using second-order Mur boundary conditions. This spacing was sufficient for cell sizes ranging from about $\lambda/20\pi$ to $\lambda/2.5$. Smaller spacings were not examined because of the minimum requirements of the programmed algorithm. While it is possible that models requiring larger spacings may exist, this six to nine cell approximation provides a good starting approximation for the minimum spacing between the target and the absorbing boundary.

C. Elimination of Field Storage in Shielded Internal Volume

Many RCS targets are largely made up of metal, which may be assumed to be a perfect conductor at high frequencies. Since the electromagnetic fields inside a perfect conductor are zero, many of the FDTD cells in models of RCS targets contain zero field values. There is no need to store and compute these fields using FDTD, because they are always zero. Slight improvement in the numerical accuracy and stability of the algorithm is in fact achieved by defining fields in these cells to be zero rather than trying to compute them as infinitely small values. Substantial savings in storage can be achieved by not storing field values in these cells.

27	28	29	30	31	32
21	22	23	24	25	26
17	18	0	0	19	20
13	14	0	0	15	16
7	8	9	10	11	12
1	2	3	4	5	6

Fig. 5. Linear indexing scheme for elimination of field storage in shielded internal volume ($2\Delta \times 2\Delta$ square metal cylinder embedded in $6\Delta \times 6\Delta$ total volume).

A simple algorithm to eliminate storage of the fields in the shielded internal volume where they are known to be zero is now described. A single-dimensioned integer array of length N_{xyz} is established, where N_{xyz} is the total number of FDTD cells. This array is filled with integers assigning a cell number to each cell. The cell number is incremented for every cell until a "metal" cell is reached, and the cell number for any "metal" cell is assigned as 0. The indexing scheme for a simple square scatterer is shown in Fig. 5. The storage savings are achieved because the field components (six in three dimensions, three in two dimensions) in each cell can now be stored in single-dimensioned arrays dimensioned from 0 to N_{nm}, where N_{nm} is the number of nonmetal cells, instead of the traditional three-dimensioned arrays with a total length of N_{xyz}. Field values in the 0 index are always defined to be 0.0, and field values in the other indices are calculated using FDTD. This algorithm was used for all of the two-dimensional test cases shown above. This algorithm does not change the FDTD computed field values (assuming that fields have always been assigned to be zero in appropriate cells), because only the indexing scheme used to store the field values is changed, not the values or the computations themselves.

The storage savings in three dimensions is given by

$$\text{savings(bits)} = 6 * R_{\text{bits}} * N_m - I_{\text{bits}} * N_{xyz} \qquad (3)$$

where R_{bits} is the number of bits used to represent real numbers, I_{bits} is the minimum number of bits which can be used to represent the integer array, N_m is the number of "metal" cells, and N_{xyz} is the total number of FDTD cells. The first term in (3) is the savings from not storing real field arrays in "metal" cells, and the second term is the additional overhead from the indexing array. For example, with 3.5 megawords of memory, a metal cube can be modeled with 64 cells on a side in a model 78 cells on a side. The total model was 474552 cells, 262144 of which are "metal." If real words are represented by $R_{\text{bits}} = 32$, and the indexing array is represented by $I_{\text{bits}} = 19$, then a savings of 41315160 bits will be observed. This is equivalent to 1291098 real words, which would allow

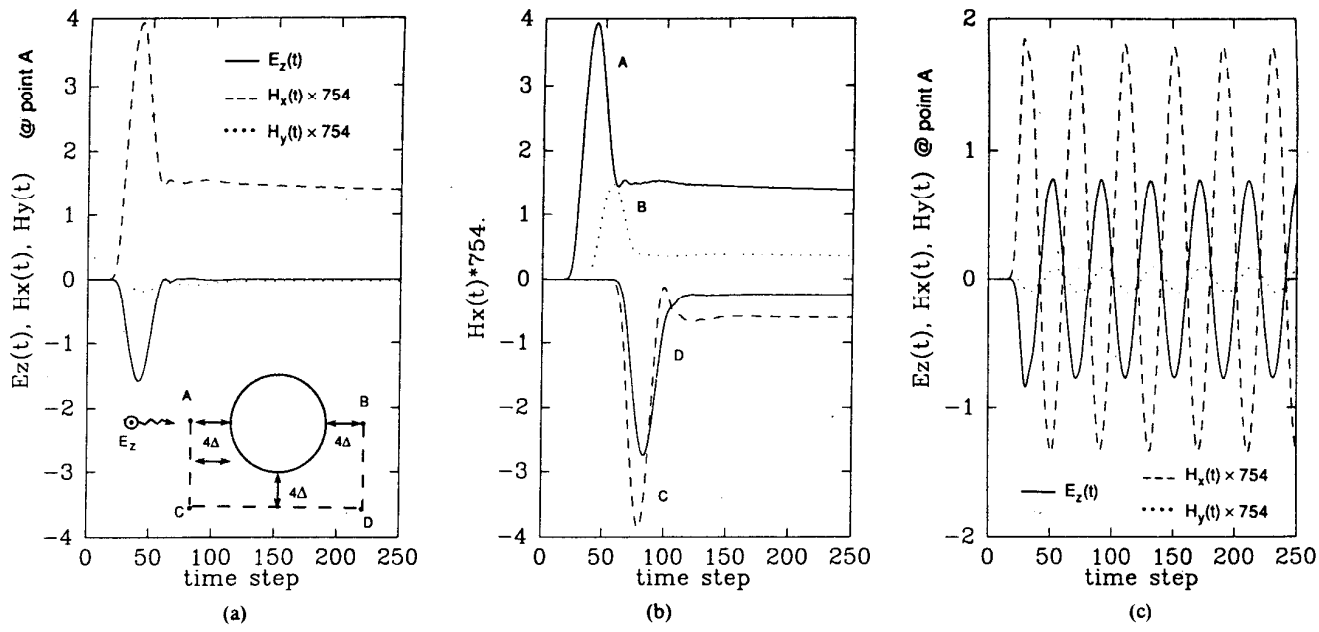

Fig. 6. The dc offset in $H_x(t)$ component for circular, perfectly conducting infinite cylinder (TM polarization). Incident field is 1 V/m raised cosine pulse, $F_b = 4$ GHz, $\Delta x = \lambda_{min}/20 = 0.375$ cm, radius $= 10\Delta x = 0.0375$ m. H_x and H_y are shown normalized by 754. (a) $E_z(t), H_x(t), H_y(t)$ at point A showing dc offset in pulse calculations. (b) $H_x(t)$ at points A, B, C, D showing spatial variation of offset. (c) $E_z(t), H_x(t), H_y(t)$ at point A showing dc offset in CW calculations ($f = 4$ GHz).

modeling of an additional 215 183 *nonmetal* cells, or a cube 75 cells on a side with a total model 89 cells on a side. A model of this size without the storage savings achieved by eliminating the shielded internal volume of the cube would require about 8.75 megawords of memory (estimated), about 2.5 times as much as with this storage savings. This represents a substantial savings in storage for a relatively simple change in programming, minimal additional computational time, and no loss of accuracy.

Special consideration must be given to the cells on the surface of the scatterer to determine if these cells are "metal" cells. To be considered a "metal" cell, all of the field components within the cell must be zero. In the traditional FDTD algorithm, field components are dispersed throughout the cell [6]. For example, in two-dimensional FDTD with TM polarization, the fields on the surface of the cell are H_{normal} and $E_{tangential}$, which are zero on the surface of a perfect conductor. In the case of TE polarization, however, the fields on the surface of the cell are $H_{tangential}$ and E_{normal}, which are not zero. For TE polarization, the shielded internal volume is taken to be one cell inside the scatterer.

The large amount of memory required for computing the RCS of realistic targets has been a continual challenge for FDTD. The use of maximum cell size, minimum number of external cells, and this new method to eliminate field storage in the shielded internal volume of perfectly conducting targets can significantly increase the size of the targets which can be modeled using the FDTD algorithm.

IV. *H* Field dc Offset

The use of FDTD for calculation of the RCS's of perfectly conductive targets is subject to yet another unique problem. The surface currents induced on the perfect conductor by the incident time-varying fields do not decay with time, as there is no dissipative mechanism. These currents then induce a magnetic field in the near field of the target. If this near zone dc magnetic field is then sampled and transformed to the far field for RCS calculations, it makes these calculations appear to be nonconvergent, even though the electric and magnetic fields converge very well. In this section, the dc magnetic field computed by FDTD calculations is illustrated, its complicating effect on RCS calculations is demonstrated, and methods to remove its effect are presented. RCS calculations in Sections II and III were made with the effect of dc magnetic field removed.

This dc offset is illustrated for the circular metal cylinder with $\Delta x = \lambda_{min}/20$ presented in Section II. The backscattered RCS of this cylinder calculated using FDTD is shown in Fig. 3. A 1 V/m TM polarized raised cosine plane wave with $F_b = 4$ GHz is incident from the $+y$ direction. The electric and magnetic fields at point A are shown in Fig. 6(a). H_x has a notable dc offset, and all field components show good convergence. The magnitude of the dc offset is not uniform throughout the problem space, as can be seen from Fig. 6(b). This figure shows H_x fields at four points surrounding the cylinder. The magnitudes of the dc offsets vary from 0.33 to 2.0 mA. The offset in fact decays approximately exponentially away

from the target. The dc offset also appears for CW excitation. Fig. 6(c) shows the fields at point A for the cylinder described above illuminated by a 4 GHz sinusoidal plane wave. The dc offset again appears in the H_x field component, and all fields converge very well.

In two dimensions, the dc offset is observed only for TM illumination of highly conductive objects. In three dimensions, the dc offset is observed for both TE and TM illumination of highly conductive objects. The offset is not observed for scattering from imperfectly conducting dielectrics. These observations are consistent with the understanding that the dc magnetic field is induced by surface currents.

The transformation of near fields containing this static magnetic field makes the frequency-domain solutions appear to be oscillatory even when the time-domain fields converge satisfactorily. Fig. 7 shows the time-domain H_x field at point A (as also shown in Fig. 6(a)) and the computed real and imaginary frequency-domain fields as a function of time. The computed values of both the real and imaginary frequency-domain fields oscillate around the correct value but do not converge to it. When the computed frequency-domain values are oscillatory, the computed RCS is also oscillatory.

The oscillatory behavior of frequency-domain calculations can be explained by breaking the summation in (2) into two separate summations, one over the nonconstant portion of the pulse (up to $n1$), the other over the constant portion of the pulse where the complex exponential is represented as a complex sinusoid as shown in

$$G(k\Delta f)=\Delta t\left\{\sum_{n=0}^{n1} g(n\Delta t)\exp\left(\frac{2\pi kn}{N}\right)+\sum_{n=n1+1}^{N-1} g(n1)\cdot\left[\cos\left(\frac{2\pi kn}{N}\right),-\sin\left(\frac{2\pi kn}{N}\right)\right]\right\}. \quad (4)$$

The first term in (4) gives the average (and desired) value of $G(k\Delta f)$, and the second term gives the oscillatory nature of the calculated results. The value of the first term cannot easily be extracted in this application, because the field values throughout the grid converge at different times. By the time convergence has been observed, the value of the first term has been overestimated in partial calculation of the second term. A more feasible way of obtaining the average is to observe that the second term is a sum of sinusoids, and hence is also a sinusoid, with frequency $k\Delta f$ and amplitude $g(n1)N/2\pi k$. The real part oscillates as a sine wave, and the imaginary part oscillates as a cosine wave with phase = 0 at time = 0. Since the form of $G(k\Delta f)$ is now known, its average value can be calculated at any time step beyond $n1$. No additional storage is required for these calculations.

This oscillation in the frequency-domain calculations caused by the dc offset in the magnetic field can be removed from CW calculations by averaging the positive and negative peaks of the steady-state sinusoid. With the effects of the dc offset removed from either CW or pulsed FDTD calculations by postprocess averaging, the calculated RCS does converge to the correct value, which is shown in Fig. 3. All test cases in this study were performed with postprocess adjustment for the magnetic field dc offset.

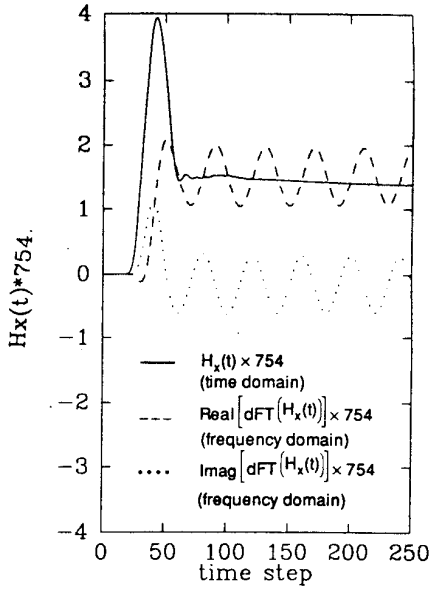

Fig. 7. $H_x(t)$ (time domain) and resultant calculated frequency domain at point A, showing oscillation induced by dc offset on frequency-domain field calculation for circular, perfectly conducting infinite cylinder (TM polarization). Incident field is 1 V/m raised cosine pulse, $F_h = 4$ GHz, $\Delta x = \lambda_{min}/20 = 0.375$ cm, radius $= 10\Delta x = 0.0375$ m. Frequency-domain values are shown for 4 GHz, and all values are shown multiplied by 754.

V. Summary and Conclusions

Several improvements to the FDTD method for calculating the RCS of a perfectly conducting target have been presented in this paper. CW and pulsed excitations for FDTD were compared, and it was shown that pulsed FDTD was by far the more efficient method for computing the frequency response of targets. Both methods had virtually identical storage requirements and gave virtually identical results. Methods to minimize FDTD storage requirements were discussed. The maximum usable cell size was examined in order to minimize the number of cells required to model a target. It was found that cell sizes as low as $\lambda_{min}/5$ were sufficient to model square bodies, sizes of $\lambda_{min}/10$ to $\lambda_{min}/20$ were sufficient to model curved bodies with TM polarization, and sizes of $\lambda_{min}/20$ to $\lambda_{min}/30$ were sufficient to model curved bodies with TE polarization using the traditional FDTD algorithm. The minimum spacing between the target and the absorbing boundary was also discussed, and it was found that six to nine cells provided sufficient spacing using second-order Mur boundary conditions with cell sizes ranging from $\lambda/20\pi$ to $\lambda/2.5$. A new method to

eliminate field storage in the shielded internal volume of perfect conductors was also presented and shown to provide substantial storage savings. The magnetic field dc offset induced by surface currents on perfect conductors was examined and was observed to make the FDTD frequency-domain calculations and hence RCS calculations oscillatory. Postprocess averaging methods were presented to remove the effects of this dc offset for both CW and pulsed FDTD, and resultant stability in the RCS calculations was achieved.

REFERENCES

[1] J.-Y. Chen and O. P. Gandhi, "Electromagnetic deposition in an anatomically based model of man for leakage fields of parallel-plate dielectric heater," *IEEE Trans. Microwave Theory Tech.*, vol. 37, pp. 174–180, Jan. 1989.

[2] C.-Q. Wang and O. P. Gandhi, "Numerical simulation of annular phased arrays for anatomically based models using the FDTD method," *IEEE Trans. Microwave Theory Tech.*, vol. 37, pp. 118–126, Jan. 1989.

[3] X. Zhang, J. Fang, K. K. Mei, and Y. Liu, "Calculations of the dispersive characteristics of microstrips by the time-domain finite difference method," *IEEE Trans. Microwave Theory Tech.*, vol. 36, pp. 263–267, Feb. 1988.

[4] T. Shibata, T. Havashi, and T. Kimura, "Analysis of microstrip circuits using three-dimensional full-wave electromagnetic field analysis in the time domain," *IEEE Trans. Microwave Theory Tech.*, vol. 36, pp. 1064–1070, June 1988.

[5] K. S. Kunz and K.-M. Lee, "A three-dimensional solution of the external response of an aircraft to a complex transient EM environment. Part I—The method and its implementation," *IEEE Trans. Electromagn. Compat.*, vol. EMC-20, pp. 328–333, 1978.

[6] A. Taflove and K. Umashankar, "Review of FD-TD numerical modelling of electromagnetic wave scattering and radar cross section," *Proc. IEEE*, vol. 77, pp. 682–698, May 1989.

[7] K. Umashankar and A. Taflove, "A novel method to analyze electromagnetic scattering of complex objects," *IEEE Trans. Electromagn. Compat.*, vol. EMC-25, pp. 433–440, 1983.

[8] G. Mur, "Absorbing boundary conditions for the finite-difference approximation of the time-domain electromagnetic-field equations," *IEEE Trans. Electromagn. Compat.*, vol. EMC-33, pp. 377–382, 1981.

[9] R. J. Leubbers, F. P. Hunsberger, and K. S. Kunz, "FDTD formulation for frequency dependent permittivity," presented at IEEE Antennas and Propagation Society Int. Symp., San Jose, CA, June 26–30, 1989.

[10] T. G. Moore and A. Taflove, "FD-TD numerical modeling of electrically large 3-D structures, both bare-metal and RAM-loaded," presented at IEEE Antennas and Propagation Society Int. Symp., San Jose, CA, June 26–30, 1989.

[11] C. V. van de Hulst, *Light Scattering by Small Particles*. New York: Dover, 1981, p. 371.

[12] T. G. Moore, J. G. Blaschak, A. Taflove, and G. A. Kriegsmann, "Theory and application of radiation boundary operators," *IEEE Trans. Antennas Propagat.*, vol. 36, pp. 1797–1811, Dec. 1988.

[13] M. G. Cote, M. B. Woodworth, and A. D. Yaghjian, "Scattering from a perfectly conducting cube," *IEEE Trans. Antennas Propagat.*, vol. 36, pp. 1321–1329, Sept. 1988.

[14] N. K. Madsen and R. W. Ziolkowski, "Numerical solution of Maxwell's equations in the time domain using irregular nonorthogonal grids," *Wave Motion*, vol. 10, pp. 583–596, Dec. 1988.

Cynthia M. Furse was born in Stillwater, ME, on May 7, 1963. She received the B.S.E.E. degree with a mathematics minor and the M.S.E.E. degree from the University of Utah in 1986 and 1988, respectively.

She was a summer research engineer with the Chevron Oil Field Research Company in 1986, and since then has been a research assistant at the University of Utah. She is currently pursuing the Ph.D. degree in electrical engineering there and is a recipient of Educational Fellowships from the IEEE Microwave Theory and Techniques Society for 1989 and 1990. Her research interest is numerical modeling of wave propagation and scattering in complex media.

Satnam P. Mathur (M'88) was born in Dholpur, India, in 1943. He received the Diploma in electronics and radio engineering (with honors) from BTE, Bombay, India, in 1966. From 1966 to 1967 he served as Scientific Assistant in the Microwave Division at the Tata Institute of Fundamental Research, Bombay. He received the M.A.Sc. degree in electrical engineering from the University of Windsor, Windsor, Canada, in 1969 and the Ph.D. degree in electrical engineering from Michigan State University, East Lansing, in 1974.

From 1974 to 1975 he was with the School of Radar Studies at the Indian Institute of Technology, New Delhi. From 1975 to 1982 he was an Assistant Professor and from 1982 to 1987 a Professor of Electrical Engineering at the Delhi College of Engineering, Delhi University, India. In 1988 he became a Research Associate at the University of Utah, Salt Lake City. Currently he is with the ERC BioServices Corporation, where he is engaged in microwave hazard research.

Dr. Mathur is a coauthor of the book *Electronic Devices, Applications and Integrated Circuits*.

Om P. Gandhi (S'57–M'58–SM'65–F'79) is a Professor of Electrical Engineering at the University of Utah, Salt Lake City. He is the author or coauthor of several book chapters, over 200 journal articles on microwave tubes, solid-state devices, and electromagnetic dosimetry, and the textbook *Microwave Engineering and Applications* (New York: Pergamon).

Dr. Gandhi received the Distinguished Research Award from the University of Utah for 1979–1980 and a special award for "Outstanding Technical Achievement" from the IEEE, Utah Section, in 1975. He is Cochairman of the ANSI C95.4 Subcommittee on the RF Safety Standards (1988–) and a past Chairman of the IEEE Committee on Man and Radiation (COMAR). His name is listed in *Who's Who in the World*, *Who's Who in America*, *Who's Who in Engineering*, and *Who's Who in Technology Today*.